Fermilab FERMILAB-Conf-99/383-E D0 June 2000

A large statistics study of the performance and yields of generation-6 VLPCs (HISTE-VI)

D. Lincoln (for the DØ Collaboration, Central Fiber Tracker Group)

Fermi National Accelerator Laboratory, P.O Box 500, Batavia, IL 60510, USA

In this paper, the DØ collaboration reports on the test results of 142 880 VLPC pixels. We have explored the space of operating conditions and find good performance at a temperature of 9 K and an average bias voltage of 7 V. Preliminary tests have shown an average quantum efficiency of 80% and a gain of 20 000 – 60 000. Tests have shown that the devices can be made to work at very high rates. The pixel-to-pixel variation within a chip is manageable, allowing one to assemble like-performing VLPC chips into cassettes containing 1024 pixels each.

The DØ experiment is currently embarked on an ambitious upgrade [1] of its central tracking system. The earlier tracker has been removed and is being replaced by a super-conducting solenoid magnet, a large silicon vertex detector and an innovative tracker consisting of scintillating fibers. Each scintillating fiber is read out by an individual Visible Light Photon Counter (VLPC). These devices are solid-state photodetectors consisting of layers of doped and undoped silicon [2]. They have been previously used in a much smaller context [3]. In the HISTE-VI model, each VLPC pixel has a 1mm diameter circular shape, well matched for our scintillating fiber. The pixels are arranged in a 2×4 array on a chip. These chips are then soldered to an aluminum nitride substrate. The chip is connected to pads on the substrate with gold wire. These pads allow electrical access to the VLPCs. VLPC chips are epitaxially grown on 3.5" diameter wafers (176 chips/wafer). Twelve different loadings of the reactor, each containing 21 wafers, were needed to provide enough VLPCs for DØ.

Earlier publications [4] have described the general properties and operating conditions of VLPCs and the techniques used to test them. This proceeding is intended to update the results presented in these earlier publications. The data set presented here comprises 17860 tested hybrids, with 15825 successfully passing. We are currently reworking and retesting the failed chips, with a recovery rate on the order of 50%.

Fig. 1 shows the signal distribution of a VLPC pixel when operating with no light illuminating it and also with a low level of illumination. The individual photoelectron (pe) peaks are clearly evident. When no light is present, one occasionally observes a single electron in the gate of the ADC, generated by thermal processes. When VLPCs are run at temperatures above their nominal operating point (6-12 K, depending on operating voltage), the rate of thermal electrons (or internally generated noise) is much increased and the single pe peak becomes more pronounced.

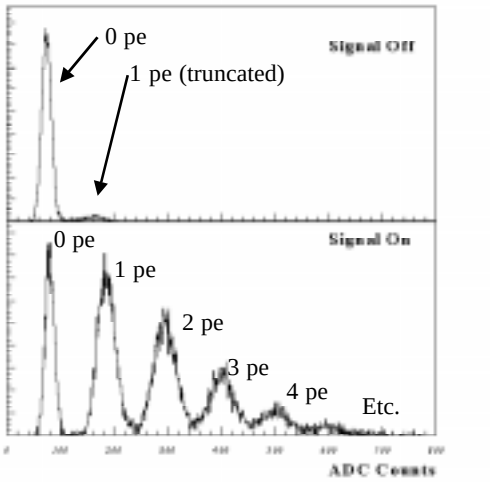

Figure 1 Typical signal distributions with and without an active light source.

The test suite for VLPCs is described in Ref. 4, but the basic idea is that we choose an operating temperature that gives good gain and quantum efficiency characteristics, while minimizing thermal noise. This temperature was 9 K. We then tested the VLPCs by illuminating them with

two LEDs, one flashing at a rate which simulates the minimum bias rate expected in the DØ environment, the other flashing at a rate more characteristic of the expected trigger rate. We then changed the operating voltage, noting its effect on the predicted trigger efficiency for DØ. The voltage at which this efficiency was maximized was taken to be the optimum operating voltage. The distribution of these voltages is shown in Fig. 2.

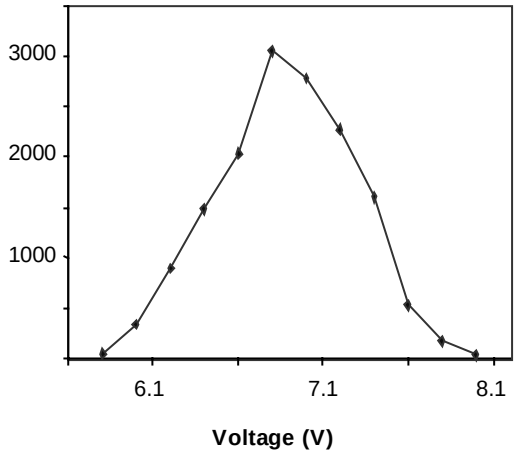

Figure 2 Optimum operating voltage distribution for VLPCs.

While the gain of the VLPCs is dependent on both the temperature and voltage, the gain at the operating voltage is a well-defined measure of the performance of the device. The distribution of these gains is given in Fig. 3. There are three curves (left, right and the sum of the two). The right curve shows the gain distribution for the first four reactor loadings (1/3 of the chips). The left curve shows the gain distribution for the remaining eight reactor loads, which occurred six months later. During this time, the reactor was disassembled, moved and reassembled. In addition, an attempt was made to modify the chip growth parameters in order to increase the difference between the desired operating voltage and the voltage at which the chip underwent breakdown (a Geiger-like mode, characterized by huge pulses at a fast rate). While the slight changes in chip growth parameters successfully suppressed the onset of breakdown, it had the deleterious effect of reducing the overall gain.

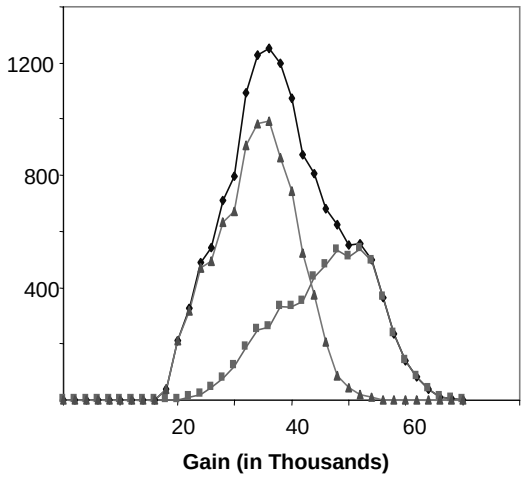

Figure 3 Gain distributions for early reactor loads (right), late ones (left) and all chips (top).

The RMS of the gain distribution is on the order of 25-30%, dominated by the fact that each chip is operating at a separate voltage. Within the eight pixels that constitute a chip, the uniformity is much better. The distribution of gain RMS within a chip is shown in Fig. 4. Inter-pixel variation is on the order of 1.5%. In this plot, the amplifier variations have not been removed.

Earlier we alluded to the gain variation as a function of operating voltage. The variation is demonstrated in Fig. 5. In Fig. 5a, we show the gain as a function of voltage. The horizontal axis is the difference from the operating voltage. The error bars are RMS, not standard error, showing the large variation in gain. The error on the mean is negligible. There are two sets of data represented: one with the background LED turned off (0 MHz), consistent with very low luminosity running and the other with a high rate background LED (20 MHz) approximately a factor of three above the background rate expected to be

observed in the inner layers of the DØ fiber tracker at an experimental luminosity of 2×10^{32} $cm^{-2}s^{-1}$. The specified rates refer to the pe rate incident on a VLPC pixel. The operating voltages are different at the two background rates, with the higher background rate corresponding typically to a 0.5V higher operating voltage.

In Fig. 5b, we remove the chip-to-chip gain variation and plot instead the fractional gain, normalized to the gain at the operating voltage. The error bars still represent the RMS. We see that the fractional gain is well-determined by the operating voltage. Thus, given the gain at any voltage, one can predict the gain at any other voltage with an accuracy on the order of 2-3%.

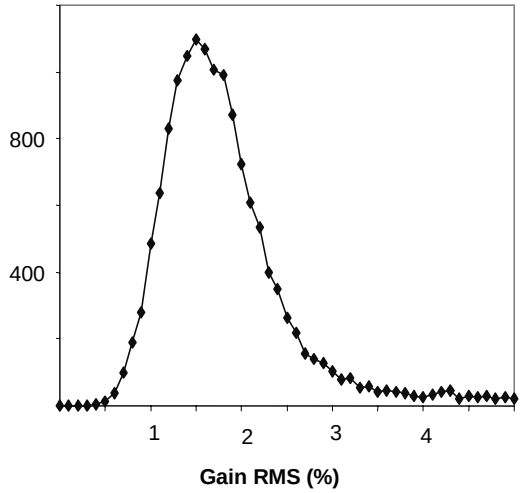

Figure 4 Gain RMS distribution at operating voltage.

Two additional important operating parameters are the quantum efficiency and the noise, both of which are functions of temperature, operating voltage and background rate. In Fig. 6, we present these variables at a temperature of 9K as a function of voltage for two background rates.

Fig. 6a shows the quantum efficiency as a function of voltage, referenced from the operating voltage. The absolute quantum efficiency is not well known, thus the vertical axis is somewhat arbitrary. We normalize it to plateau at 80%, a

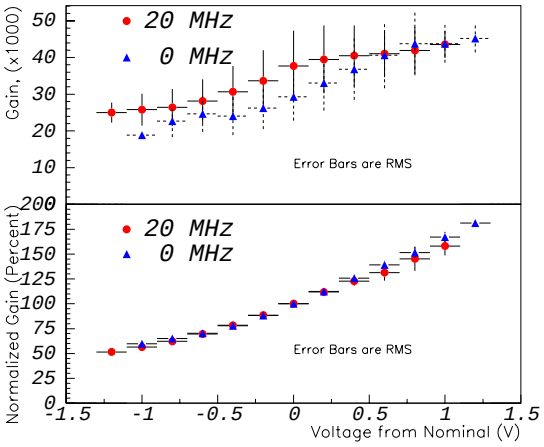

Figure 5 (a) Gain and (b) fractional gain (in %), as a function of voltage, referenced from the operating voltage.

value suggested by the manufacturer. An independent verification of this number is planned. We see that for both background rates the curves are quite similar. While the absolute numbers are uncertain, we may say that at the higher operating voltage characteristic of higher background rates, one achieves a quantum efficiency that is a few percent higher than that achieved at low background rates, with an RMS of 5%.

Fig. 6b shows the noise threshold in units of photoelectrons. Noise threshold is defined to be the point at which one may set a threshold that is exceeded only a 0.5% of the time. Fig. 6 shows two striking features. First, the operating voltage chosen by our algorithm is not on the quantum efficiency plateau. Second, the noise increases dramatically after the operating voltage. Our algorithm tries to maximize the trigger efficiency achieved in the collider environment. Because gain, quantum efficiency and noise are all correlated with the voltage (our primary adjustable parameter), we are not able to simultaneously independently optimize all three variables. We see that if we exceed the operating voltage by a small amount, we increase the signal only a small amount, while the noise rate increases more rapidly. Because the error bars

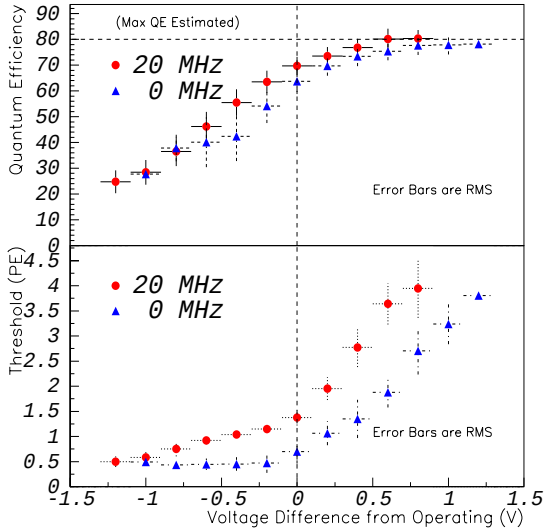

Figure 6 (a) Quantum efficiency and (b) threshold as a function of voltage. In both cases the operating voltage is the reference.

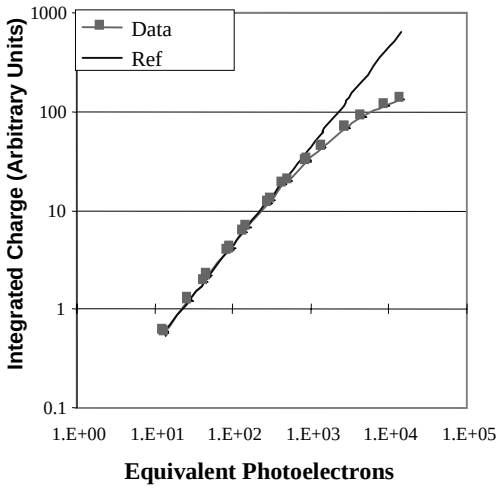

Figure 7 Linearity behavior of a high-gain VLPC.

shown are the RMS, we observe that the various chips are quite similar in these variables.

The actual behavior of the threshold as a function of the operating voltage is exponential, a behavior not observed in Fig. 6. This is because our amplifier added a width to our single pe peaks of 10-20% of the inter-peak separation, depending on gain. Consequently, the low-voltage threshold plateau at 0.5 pe is explained by this amplifier width.

Fig. 7 shows the linearity behavior of a particular VLPC pixel. This behavior is quite typical, with only a slight dependence on gain, operating voltage, or noise characteristics. In this measurement, an ultraviolet laser (λ=337 nm) was used to illuminate a piece of scintillator, doped with green wavelength shifter. The resultant light was directed towards a small number of VLPCs. The light was then attenuated using neutral density filters, so that the light range varied over five orders of magnitude (1-5×10^4 pe). Since we are unable to determine whether the cause of the loss of linearity is from loss of quantum efficiency or loss of gain, we plot on the horizontal axis equivalent photoelectrons. This is the number of photons incident on the VLPC, multiplied by the quantum efficiency for low number of photons (near 80%).

The VLPCs become nonlinear by approximately 10% at 600 equivalent photoelectrons. This is consistent with results published for an earlier version of the VLPCs (HISTE-IV) [5].

VLPCs have proven themselves to be a very successful photodetector technology. They are high rate, high gain, high quantum efficiency and low noise devices which are well matched for use in scintillating fiber applications.

[1] S. Abachi et al., FERMILAB-PUB-96-357-E.

[2] G.B. Turner et al., proceedings of SCIFI93, 1995; M.G. Stapelbroek and M.D. Petroff, ibid.

[3] M. Ambrogiani et al., IEEE Trans. Nucl. Sci. 44 (1997) 460; R. Mussa et al., Nucl. Instrum. Meth. A 360 (1995) 13.

[4] D. Lincoln, Nuclear Physics B (Proc. Suppl.) 78 (1999) 281; A. Bross et al., to be published in the proceedings of the Fifth International Conference on Position Sensitive Detectors.

[5] A. Bross et al., Nucl. Instrum. And Meth. A, 394 (1997) 87.